Inorganic Chemistry

pubs.acs.org/IC Article

$CaCu_3Mn_2Te_2O_{12}$: An Intrinsic Ferrimagnetic Insulator Prepared Under High Pressure

Haoting Zhao, Yujie Bai, Kang Yin, Xiao Wang, Zhehong Liu, Xubin Ye, Dabiao Lu, Jie Zhang, Maocai Pi, Zhiwei Hu, Hong-Ji Lin, Chien-Te Chen, Qingbo Meng, Pu Yu, Qinfang Zhang,* and Youwen Long*

Cite This: *Inorg. Chem.* 2023, 62, 21233−21239 Read Online

ACCESS | Metrics & More | Article Recommendations

ABSTRACT: $CaCu_3Mn_2Te_2O_{12}$ was synthesized using high-temperature and high-pressure conditions. The compound possesses an A- and B site ordered quadruple perovskite structure in $Pn\bar{3}$ symmetry with the charge combination of $CaCu_3^{2+}Mn_2^{2+}Te_2^{6+}O_{12}$. A ferrimagnetic phase transition originating from the antiferromagnetic interaction between A′ site Cu^{2+} and B site Mn^{2+} ions is found to occur at $T_C \approx 100$ K. $CaCu_3Mn_2Te_2O_{12}$ also shows insulating electric conductivity. Optical measurement demonstrates the energy bandgap to be about 1.9 eV, in agreement with the high B site degree of chemical order between Mn^{2+} and Te^{6+}. The first-principles theoretical calculations confirm the $Cu^{2+}(\downarrow)-Mn^{2+}(\uparrow)$ ferrimagnetic coupling as well as the insulating nature with an up-spin direct bandgap. The current $CaCu_3Mn_2Te_2O_{12}$ provides an intriguing example of an intrinsic ferrimagnetic insulator with promising applications in advanced spintronic devices.

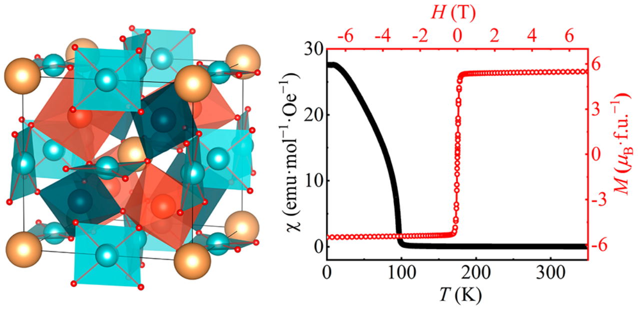

1. INTRODUCTION

Ferromagnetic or ferrimagnetic insulators, which in principle transport only spin momentum but no charge carries, have received much attention owing to potential applications in dissipationless electronic and spintronic devices,[1−4] solid-state quantum computing,[5] and magnetic tunneling junctions.[6,7] As is well-known, ferromagnetism usually originates from the double exchange mechanism or Ruderman−Kittel−Kasuya−Yosida interaction,[8,9] which typically leads to metallic conductivity. Therefore, ferromagnetism and insulation are often incompatible in a single-phase material. As a result, the amount of intrinsic ferromagnetic insulators without chemical substitution is limited.[10−12] Thus far, the reported intrinsic ferromagnetic insulators mainly include europium chalcogenides (EuO, EuS),[13,14] 2D van der Waals materials of chromium trihalides (CrI_3, $CrBr_3$)[15,16] and ternary chromium trihalides ($Cr_2Si_2Te_6$, $Cr_2Ge_2Te_6$),[17,18] perovskite-type materials ($BiMnO_3$, La_2NiMnO_6, Ba_2NiOsO_6, Ba_2NaOsO_6),[11,19−21] and garnets ($Y_3Fe_5O_{12}$).[22] Although a few ferromagnetic insulators like $Y_3Fe_5O_{12}$ and La_2NiMnO_6 have higher Curie temperatures (T_C), most of them have relatively low values of T_C. For example, the T_C is only about 6.8 K for Ba_2NaOsO_6, 16 K for EuS, and 33 K for $Cr_2Si_2Te_6$.[17,23] Moreover, the 2D van der Waals ferromagnetic insulators are usually unstable under ambient conditions. Since a wide energy bandgap E_g (e.g., > 1.0 eV at room temperature) can effectively prevent charge carriers from thermal excitation, in addition to a relatively high T_C, a considerable E_g is also desirable for possible applications of ferromagnetic insulators.

Both A- and B site ordered quadruple perovskite oxide with chemical formula $AA'_3B_2B'_2O_{12}$ provides a unique opportunity to design intrinsic ferromagnetic or ferrimagnetic insulators. First, $AA'_3B_2B'_2O_{12}$-type quadruple perovskite crystallizes into a $Pn\bar{3}$ space group with $A'O_4$ square-planar and $B/B'O_6$ octahedral units (see Figure 1a). In this peculiar structure, the A site is usually occupied by a larger alkali metal, alkaline earth, or rare earth ion, while the A′ site is usually occupied by a smaller-size transition metal ion with strong Jahn−Teller effect like Cu^{2+} and Mn^{3+}. In addition, transition metal ions also occupy the B and B′ sites in an orderly manner. Since three different atomic sites (A′, B, and B′ sites) can accommodate transition metals, multiple magnetic and electrical interactions are formed via A′−A′, A′−B/B′, and B−B′ pathways, which are beneficial to a high T_C. An interesting example is the half metal of $LaCu_3Fe_2Re_2O_{12}$, which

Received: September 19, 2023
Revised: November 20, 2023
Accepted: November 22, 2023
Published: December 13, 2023

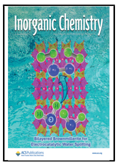

https://doi.org/10.1021/acs.inorgchem.3c03288
Inorg. Chem. 2023, 62, 21233−21239

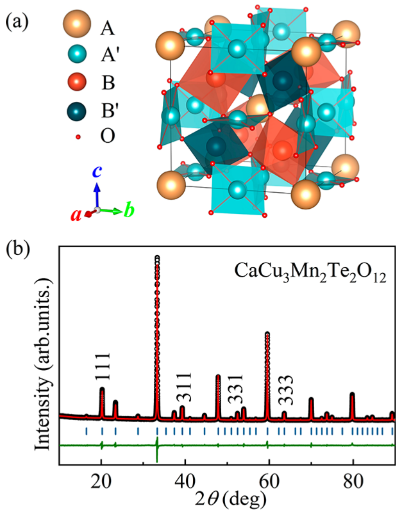

Figure 1. (a) Crystal structure of both A and B site ordered quadruple perovskite oxide $AA'_3B_2B'_2O_{12}$. The square-planar $A'O_4$ units and corner-sharing BO_6 and $B'O_6$ octahedra are shown. (b) XRD pattern and refinement results for $CaCu_3Mn_2Te_2O_{12}$ at RT. The observed (black circle), calculated (red line), and difference (olive line) values are shown. The ticks indicate the allowed Bragg reflections with space group $Pn\bar{3}$.

has the highest $T_C \approx 710$ K among all of the perovskite oxides.[24] Therefore, it is possible to find a high T_C in $AA'_3B_2B'_2O_{12}$-type quadruple perovskite. Second, the electrical transport properties of these perovskites can be manipulated through the design of element and charge combinations of B and B′ ions due to the corner-sharing BO_6 and $B'O_6$ octahedra. For example, the presence of diamagnetic ions with fully filled d orbitals (d^{10}) at B or B′ sites can improve insulating electric conductivity with a considerable E_g. In this study, an $AA'_3B_2B'_2O_{12}$-type quadruple perovskite oxide of $CaCu_3Mn_2Te_2O_{12}$ was designed and synthesized using high-pressure techniques. The crystal structure, charge state, specific heat, and magnetic and electric properties were investigated in detail. The compound exhibits intriguing ferrimagnetic ($T_C \approx 100$ K) and insulating properties with a wide $E_g \approx 1.9$ eV at room temperature (RT).

2. EXPERIMENTAL SECTION

$CaCu_3Mn_2Te_2O_{12}$ polycrystalline samples were synthesized under high-temperature and high-pressure conditions. High-purity (>99.9%) CaO, CuO, MnO_2, and TeO_2 powders with a stoichiometric ratio were used as starting materials. All of these starting materials were thoroughly mixed and ground in a glovebox filled with argon. Then, the mixed powders were pressed into a platinum capsule 2.8 mm in diameter and 4.0 mm in height. The capsule was treated at 9 GPa and 1373 K for 30 min on a cubic anvil-type high-pressure apparatus. Once the heating was finished, the sample was quenched to RT, and the pressure was gradually released to ambient pressure within 9 h. Phase identification was made via powder X-ray diffraction (XRD) collected using a Huber X-ray diffractometer (Cu $K_{\alpha 1}$, 40 kV, and 30 mA) with the 2θ range from 10° to 100° with steps of 0.005° at RT. The GSAS software was used for the Rietveld refinement.[25] X-ray absorption spectroscopy (XAS) at the Cu-$L_{2,3}$ and Mn-$L_{2,3}$ edges was performed at the BL11A beamline of the National Synchrotron Radiation Research Center (NSRRC) in Taiwan. Magnetic properties were measured on a magnetic property measurement system (Quantum Design, MPMS-VSM). The magnetic susceptibility of both zero-field-cooling (ZFC) and field-cooling (FC) modes was measured under a magnetic field of 0.1 T. The isothermal magnetization was measured at 2 and 200 K between −7 and 7 T. Specific heat was measured on a physical property measurement system (Quantum Design, PPMS). A UV−vis absorption spectrum was obtained on a Shimadzu UV-2550.

All theoretical calculations were based on spin-polarized density functional theory, which was implemented in the Vienna ab initio simulations package.[26] The generalized gradient approximation with a Perdew−Burke−Ernzerhof functional was employed for structural relaxation.[27] The effective Hubbard $U = 4$ eV was adopted for the Mn-d and Cu-d orbitals.[28] The planewave cutoff energy and convergence criteria for energy and force were set to be 500 eV, 10^{-5} eV, and 0.01 eV·Å^{-1}, respectively. The Monkhorst−Pack k-point mesh of 3 × 3 × 3 was used for Brillouin zone sampling.[29] To obtain reasonable electronic and magnetic properties, the Heyd−Scuseria−Ernzerhof (HSE06) hybrid functional was adopted with the mixing exchange parameter of 0.25 and screening parameter of 0.2 Å^{-1}.[30,31] Moreover, the more reliable tetrahedron method has been adopted to calculate the density of states (DOS).[32]

3. RESULTS AND DISCUSSION

Figure 1b presents the XRD pattern measured at RT and the refinement results for $CaCu_3Mn_2Te_2O_{12}$. All diffraction peaks can be well indexed based on a cubic symmetry. No discernible impurities were found to occur in the sample. The Rietveld refinements show that $CaCu_3Mn_2Te_2O_{12}$ possesses an A site and B site ordered quadruple perovskite structure with the space group $Pn\bar{3}$ (no. 201). In this symmetry, Ca and Cu atoms occupy the 2*a* (0.25, 0.25, 0.25) and 6*d* (0.25, 0.75, 0.75) sites, respectively. Different from the 12-coordinated Ca atoms at the A site, the Cu atoms at the A′ site are located in a square-planar coordination due to the strong Jahn−Teller effect (Figure 1a).[33] The 6-coordinated Mn and Te atoms at the B and B′ sites in an orderly rock-salt-type fashion occupy the 4*b* (0, 0, 0) and 4*c* (0.5, 0.5, 0.5) sites, as revealed by the diffraction peaks with $h + k + l$ = odd, such as the (111), (311), and (331) peaks (see Figure 1b).

Table 1 lists the refined structural parameters for $CaCu_3Mn_2Te_2O_{12}$. The lattice constant we refined is $a = 7.59338(1)$ Å. The nearly unity occupancy factors for cations suggest a 1:3 ordering between the A site Ca and A′ site Cu atoms and a 1:1 ordering between the B site Mn and the B′ site Te atoms. According to the refined bond lengths, the bond valence sum (BVS) calculations give the valence state to be 1.81 for Cu and 2.09 for Mn atoms, suggesting the formation of Cu^{2+} and Mn^{2+} charge states, in agreement with the XAS measurements shown below.

To further determine the valence states of Cu and Mn, the XAS at the Cu-$L_{2,3}$ and Mn-$L_{2,3}$ edges, which are widely known to be sensitive to the valence state and local environment,[34,35] were collected. Figure 2a shows the Cu-$L_{2,3}$ edges of $CaCu_3Mn_2Te_2O_{12}$. $CaCu_3^{2+}Ti_4O_{12}$ was also presented as the reference of Cu^{2+} with similar CuO_4 square-planar coordination.[36] The energy position of $CaCu_3Mn_2Te_2O_{12}$ (931.0 eV for L_3 and 950.8 eV for L_2) is very close to that of $CaCu_3^{2+}Ti_4O_{12}$ (930.8 eV for L_3 and 950.6 eV for L_2), demonstrating that the Cu^{2+} valence state emerges in $CaCu_3Mn_2Te_2O_{12}$. The small shift may arise from the slight difference in the local environment of Cu^{2+}. The XAS at the Mn-$L_{2,3}$ edges of $CaCu_3Mn_2Te_2O_{12}$ are shown in Figure 2b together with $Mn^{2+}O$ as a Mn^{2+} reference and $LaMn^{3+}O_3$ as a Mn^{3+} reference with similar MnO_6 octahedral coordination.[37] Compared with $LaMn^{3+}O_3$, the main absorption peaks of $CaCu_3Mn_2Te_2O_{12}$ move toward lower energy by more than 1 eV. Moreover, the multiplet spectral feature and peak positions of Ca-

Table 1. Refined Structure Parameters of $CaCu_3Mn_2Te_2O_{12}$ at RT[a]

parameter	value	parameter	value
a (Å)	7.59338(1)	U_{iso} for Te1 ($100 \times$ Å^2)	0.94(2)
O_x	0.0763(4)	U_{iso} for Mn2 ($100 \times$ Å^2)	1
O_y	0.2326(2)	U_{iso} for O ($100 \times$ Å^2)	0.46(7)
O_z	0.5575(4)	d_{Ca-O} ($\times$ 12) (Å)	2.685(3)
G (2a for Ca)	0.991(8)	d_{Cu-O} ($\times$ 4) (Å)	1.973(2)
G (6d for Cu)	0.985(3)	d_{Mn-O} ($\times$ 6) (Å)	2.156(2)
G (4b for Mn1)	0.992(1)	d_{Te-O} ($\times$ 6) (Å)	1.909(2)
G (4b for Te2)	0.008(1)	∠Mn−O−Te (deg)	138.0(2)
G (4c for Te1)	0.992(1)	∠Cu−O−Mn (deg)	105.45(9)
G (4c for Mn2)	0.008(1)	∠Cu−O−Te (deg)	115.7(1)
U_{iso} for Ca ($100 \times$ Å^2)	1.2(2)	BVS (Cu)	1.81
U_{iso} for Cu ($100 \times$ Å^2)	1.53(7)	BVS (Mn)	2.09
U_{iso} for Mn1 ($100 \times$ Å^2)	1.04(4)	R_{wp} (%)	4.00
U_{iso} for Te2 ($100 \times$ Å^2)	1	R_p (%)	2.53

[a] Space group: $Pn\bar{3}$ (no. 201). Atomic sites: Ca 2a (0.25, 0.25, 0.25), Cu 6d (0.25, 0.75, 0.75), Mn 4b (0, 0, 0), Te 4c (0.5, 0.5, 0.5), and O 24h (x, y, z). The BVS values (V_i) were calculated using the formula $V_i = \sum_j S_{ij}$ and $S_{ij} = \exp[(r_0 - r_{ij})/0.37]$. The value of r_0 = 1.679 for Cu and r_0 = 1.765 for Mn. For the A′ site Cu, 4-coordinated oxygen atoms were used. For B site Mn, 6-coordinated oxygen atoms were used. G: site occupancy factor.

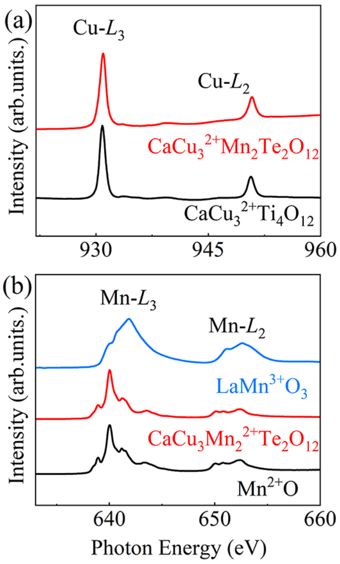

Figure 2. XAS at the (a) Cu-$L_{2,3}$ for $CaCu_3Mn_2Te_2O_{12}$ together with $CaCu_3^{2+}Ti_4O_{12}$ as the reference of Cu^{2+}. (b) Mn-$L_{2,3}$ edges for $CaCu_3Mn_2Te_2O_{12}$ together with $Mn^{2+}O$ as the reference of Mn^{2+} and $LaMn^{3+}O_3$ as the reference of Mn^{3+}.

$Cu_3Mn_2Te_2O_{12}$ are similar to those of the $Mn^{2+}O$ reference (640.0 eV for L_3 in $CaCu_3Mn_2Te_2O_{12}$ and $Mn^{2+}O$ both), indicating the formation of a Mn^{2+} valence state at the B site. For B′ site Te, the Te−O bond length (1.909(2) Å) is close to the Te^{6+}−O bond length observed in Pb_2MnTeO_6 (1.915 Å) with TeO_6 octahedral coordination,[38] suggesting the formation of a Te^{6+} charge state. Therefore, the charge combination is determined to be $CaCu_3^{2+}Mn_2^{2+}Te_2^{6+}O_{12}$.

Figure 3a displays the temperature dependence of magnetic susceptibility of $CaCu_3Mn_2Te_2O_{12}$ measured at 0.1 T. As the temperature decreases to a critical value at $T_C \approx 100$ K, both the ZFC and FC susceptibility curves experience a sharp increase, indicating the occurrence of a long-range ferromagnetic or ferrimagnetic phase transition. To identify the specific spin coupling of $CaCu_3Mn_2Te_2O_{12}$, the inverse susceptibility χ^{-1} as a function of temperature was also plotted in Figure 3a. One can find that the χ^{-1} above T_C is obviously deviated from the linear Curie−Weiss law but consistent with Néel's ferrimagnetism theory with the function $\chi^{-1}(T) = [(T - \Theta)/C] - [\xi/(T - \Theta')]$, where the first term represents the simple Curie−Weiss behavior at high temperatures, and the second term determines the hyperbolic behavior near the ferrimagnetic phase transition owing to the existence of multiple spin sublattices.[39] The data of χ^{-1} between 165 and 350 K was selected for Néel's fitting, yielding the Weiss temperature $\Theta = -133.7(8)$ K, the Curie constant C = 12.10(2) emu·K·mol^{-1}·Oe^{-1}, the fitted parameters ξ = 228(4) K·mol·Oe·emu^{-1}, and Θ' = 125.1(4) K. The negative value of Θ indicates the strong antiferromagnetic interaction in $CaCu_3Mn_2Te_2O_{12}$. The effective magnetic moment is calculated to be μ_{eff} = 9.84 μ_B·fu^{-1}, which is slightly larger than the spin-only theoretical value (8.89 μ_B·fu^{-1}) with the charge combination of $CaCu_3^{2+}Mn_2^{2+}Te_2O_{12}$. Therefore, a long-range ferrimagnetic phase transition is assigned for $CaCu_3Mn_2Te_2O_{12}$ at $T_C \approx 100$ K. Figure 3b shows the isothermal magnetization curves of $CaCu_3Mn_2Te_2O_{12}$ measured above and below the T_C. At 200 K, the linear magnetization behavior agrees well with the paramagnetic state. At 2 K, however, canonical magnetic hysteresis behavior is found to occur, further confirming the long-range ferrimagnetic ordering. With increasing field, the magnetization increases sharply and is almost saturated at 0.5 T, leading to a very small coercive field (H_C) of about 27 Oe. The specific value of saturated moment (M_S) we measured at 7 T and 2 K is 5.50 μ_B·fu^{-1}.

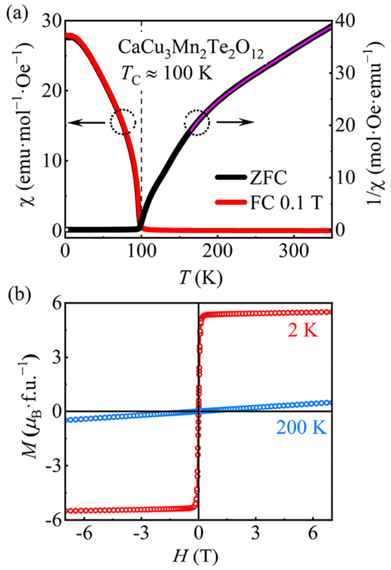

Figure 3. (a) Temperature dependence of magnetic susceptibility χ measured at 0.1 T with ZFC and FC modes (almost overlapped) and the ZFC inverse magnetic susceptibility for $CaCu_3Mn_2Te_2O_{12}$. The magenta line shows the Neel's fitting. (b) Field dependent magnetization measured at 2 and 200 K.

Figure 4a shows the temperature dependence of specific heat C_P measured at zero field for $CaCu_3Mn_2Te_2O_{12}$. In accord with the ferrimagnetic transition, a sharp λ-type anomaly is also found to occur near T_C in specific heat. To evaluate the magnetic entropy change around T_C, the Debye−Einstein model was used to fit the lattice specific heat C_{Lat}.[40] The C_p data at temperatures > 104 K were selected for C_{Lat} fitting and then the fitted curve was extended down to 2 K as the phonon background (see the black line in Figure 4a). The magnetic contribution C_{Mag} was obtained by subtracting C_{Lat} from the total C_P. As shown in Figure 4b, the magnetic entropy $\Delta S_M = \int (C_{Mag}/T)\,dT$ over the temperature range of 2−150 K was calculated to be 44.95 $J\cdot mol^{-1}\cdot K^{-1}$, which is very close to the expected value in theory with the function $3R\ln[2S(Cu^{2+}) + 1] + 2R\ln[2S(Mn^{2+}) + 1] = 47.08\ J\cdot mol^{-1}\cdot K^{-1}$, indicating that Cu^{2+} and Mn^{2+} simultaneously participate in the magnetic order. Here R is the universal gas constant, and S is the spin angular momentum. At lower temperatures (<12 K), the specific heat date can be fitted using the formula $C_P = \alpha T^3 + \beta T^{3/2}$ (see the inset of Figure 4a), where the T^3 term originates from the contribution of phonons and antiferromagnetic interactions, and $T^{3/2}$ represents the contribution of ferromagnetic excitation. The parameters obtained by the fitting are $\alpha = 1.23\ (7) \times 10^{-3}\ J\cdot mol^{-1}\cdot K^{-4}$ and $\beta = 6.3\ (4) \times 10^{-2}\ J\cdot mol^{-1}\cdot K^{-5/2}$. Note that there is no γT term contribution because of the prohibited electron conduction in $CaCu_3Mn_2Te_2O_{12}$ as shown later.

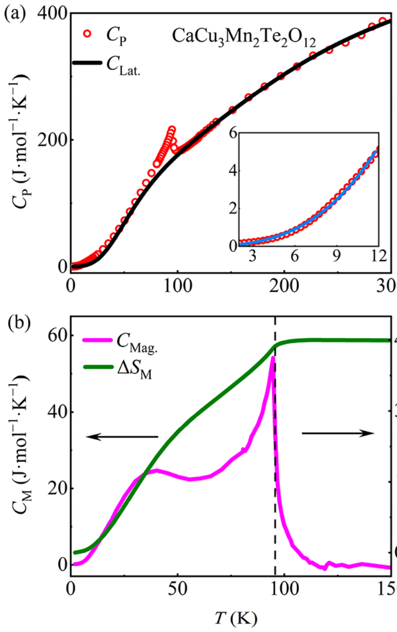

Figure 4. (a) Temperature dependence of specific heat C_P for $CaCu_3Mn_2Te_2O_{12}$ measured at zero field. The inset shows the low-temperature fitting result between 2 and 12 K using the formula $C_P = \alpha T^3 + \beta T^{3/2}$. (b) Magnetic specific heat C_{Mag} and magnetic entropy change ΔS_M around T_C.

In addition to the ferrimagnetism, $CaCu_3Mn_2Te_2O_{12}$ also exhibits insulating electric conductivity with a resistivity higher than the measurement range of PPMS (>10^5 Ω·cm at RT). The optical measurement was thus performed to characterize the electrical feature of $CaCu_3Mn_2Te_2O_{12}$). Figure 5 shows the Tauc's plot of the UV−vis absorption spectra measured at RT. According to the equation $(\alpha h\nu)^\gamma = A\,(h\nu - E_g)$, where α is the absorption coefficient, A is a proportional constant, γ is 0.5 or 2 depending on whether the bandgap is indirect or direct, and $h\nu$ and E_g denote photon energy and the optical energy bandgap, respectively.[41] The characteristic two-step-like absorption of the indirect bandgap does not appear,[42] so γ is determined to be 2 and the direct bandgap is as high as 1.9 eV. Note that the absorption below E_g shown in Figure 5 can be attributed to possible defect and/or impurity absorption. The large bandgap of $CaCu_3Mn_2Te_2O_{12}$ is beneficial for preventing charge carriers from thermal excitation. In comparison, the bandgaps of EuO and CrI_3, which are commonly used as ferromagnetic insulators in spintronics, are only 1.2 and 0.89 eV,[43,44] respectively. In addition, the thermogravimetric measurement indicates that $CaCu_3Mn_2Te_2O_{12}$ is thermally stable on heating up to 1000 K (not shown here). These features suggest that $CaCu_3Mn_2Te_2O_{12}$ is a promising intrinsic ferrimagnetic insulator for potential applications.

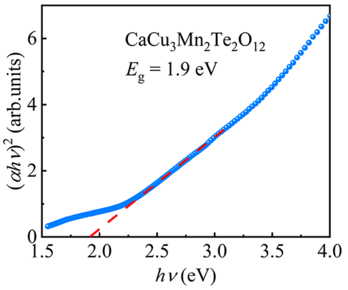

Figure 5. Tauc's plot of $(\alpha h\nu)^2$ vs $h\nu$ for $CaCu_3Mn_2Te_2O_{12}$ measured at RT.

To get deeper insight into the magnetic ground state and the electronic properties of $CaCu_3Mn_2Te_2O_{12}$, the hybrid density functional of HSE06 calculations was carried out for different collinear spin configurations. As shown in Figure 6, the calculations illustrate that the $Cu^{2+}(\downarrow)$−$Mn^{2+}(\uparrow)$ ferrimagnetic ground state as determined in experiment has the lowest energy. Actually, similar ferrimagnetic coupling was reported in isostructural compounds like $CaCu_3Cr_2Sb_2O_{12}$ and Ca-

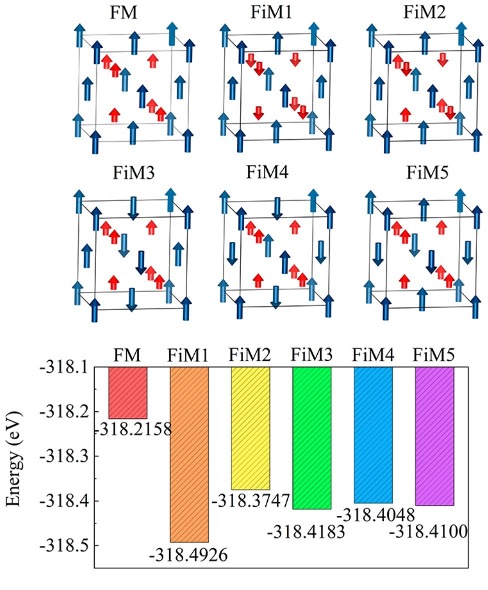

Figure 6. Schematic spin configurations considered for theoretical calculations and the related energies for $CaCu_3Mn_2Te_2O_{12}$. Blue and red arrows represent Mn and Cu spins, respectively.

$Cu_3Fe_2Nb_2O_{12}$.[45,46] In addition, the calculated magnetic moments inside the muffin-tin spheres are −0.00, −0.70, 4.54, 0.04, and −0.04 μ_B for Ca, Cu, Mn, Te, and O ions, respectively. The magnetic moments of Cu^{2+} ($S = 1/2$) and Mn^{2+} ($S = 5/2$) ions are smaller than the ideal $2S$ values owing to the hybridization with O 2p orbitals. The total magnetic moment was calculated to be 6.58 $\mu_B \cdot fu^{-1}$. This value is somehow larger than that obtained in the experiment (5.5 $\mu_B \cdot fu^{-1}$ at 2 K and 7 T). Such a difference may suggest that there is slight tilting for Cu^{2+} and/or Mn^{2+} spins in the material. Figure 7 presents the calculated electronic band structures and DOS of $CaCu_3Mn_2Te_2O_{12}$. One finds that the DOS values of the A′ site $Cu^{2+}$and B site Mn^{2+} ions considerably overlap, suggesting the strong spin interactions between these two magnetic sublattices. Moreover, the calculated E_g is 3.54 eV for the spin-down channel, while an up-spin direct E_g of 1.94 eV is observed at the Γ point, which is well consistent with the experimentally measured value (1.9 eV).

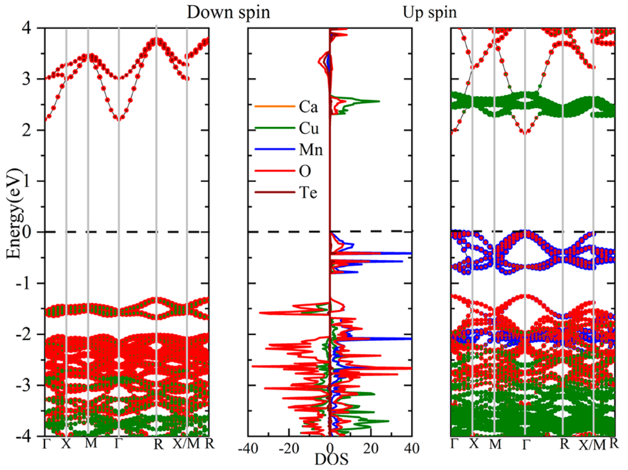

Figure 7. First-principles numerical results for the band structures and partial density of states (DOS) of $CaCu_3Mn_2Te_2O_{12}$ using HSE06.

4. CONCLUSION

In summary, the quadruple perovskite oxide $CaCu_3Mn_2Te_2O_{12}$ was successfully prepared at 9 GPa and 1373 K. The Rietveld refinement based on the powder XRD data indicates that $CaCu_3Mn_2Te_2O_{12}$ crystallize to an A and B site ordered cubic quadruple perovskite structure with space group $Pn\bar{3}$. BVS calculations and XAS measurements determine the charge combination to be $CaCu_3{}^{2+}Mn_2{}^{2+}Te_2O_{12}$. According to specific heat and magnetic susceptibility, a long-range ferrimagnetic phase transition resulting from the antiferromagnetically coupled A′ site Cu^{2+} and B site Mn^{2+} is found to occur at $T_C \approx 100$ K. In addition, $CaCu_3Mn_2Te_2O_{12}$ exhibits strong insulation with a wide E_g of 1.9 eV. The first-principles theoretical calculations further confirm the $Cu^{2+}(\downarrow)-Mn^{2+}(\uparrow)$ ferrimagnetic ground state and the insulating nature with an up-spin direct E_g. The present work provides an intrinsic ferrimagnetic insulator with promising applications in advanced spintronic devices.

■ ASSOCIATED CONTENT

Accession Codes

CCDC 2307858 contains the supplementary crystallographic data for this paper. These data can be obtained free of charge via www.ccdc.cam.ac.uk/data_request/cif, or by emailing data_request@ccdc.cam.ac.uk, or by contacting The Cambridge Crystallographic Data Centre, 12 Union Road, Cambridge CB2 1EZ, UK; fax: +44 1223 336033.

■ AUTHOR INFORMATION

Corresponding Authors

Qinfang Zhang − *Department of Physics, Yancheng Institute of Technology, Yancheng, Jiangsu 224051, China;* orcid.org/0000-0003-3233-3400; Email: qfangzhang@gmail.com

Youwen Long − *Beijing National Laboratory for Condensed Matter Physics, Institute of Physics, Chinese Academy of Sciences, Beijing 100190, China; School of Physical Sciences, University of Chinese Academy of Sciences, Beijing 100049, China; Songshan Lake Materials Laboratory, Dongguan, Guangdong 523808, China;* orcid.org/0000-0002-8587-7818; Email: ywlong@iphy.ac.cn

Authors

Haoting Zhao − *Beijing National Laboratory for Condensed Matter Physics, Institute of Physics, Chinese Academy of Sciences, Beijing 100190, China; College of Materials Science and Opto-Electronic Technology, University of Chinese Academy of Sciences, Beijing 100049, China;* orcid.org/0009-0007-9656-5709

Yujie Bai − *Department of Physics, Yancheng Institute of Technology, Yancheng, Jiangsu 224051, China;* orcid.org/0000-0001-8244-8770

Kang Yin − *Beijing National Laboratory for Condensed Matter Physics, Institute of Physics, Chinese Academy of Sciences, Beijing 100190, China; School of Physical Sciences, University of Chinese Academy of Sciences, Beijing 100049, China*

Xiao Wang − *Beijing National Laboratory for Condensed Matter Physics, Institute of Physics, Chinese Academy of Sciences, Beijing 100190, China;* orcid.org/0000-0001-8139-4192

Zhehong Liu − *Beijing National Laboratory for Condensed Matter Physics, Institute of Physics, Chinese Academy of Sciences, Beijing 100190, China*

Xubin Ye − *Beijing National Laboratory for Condensed Matter Physics, Institute of Physics, Chinese Academy of Sciences, Beijing 100190, China;* orcid.org/0000-0002-5739-8318

Dabiao Lu − *Beijing National Laboratory for Condensed Matter Physics, Institute of Physics, Chinese Academy of Sciences, Beijing 100190, China; School of Physical Sciences, University of Chinese Academy of Sciences, Beijing 100049, China*

Jie Zhang − *Beijing National Laboratory for Condensed Matter Physics, Institute of Physics, Chinese Academy of Sciences, Beijing 100190, China; School of Physical Sciences, University of Chinese Academy of Sciences, Beijing 100049, China*

Maocai Pi − *Beijing National Laboratory for Condensed Matter Physics, Institute of Physics, Chinese Academy of Sciences, Beijing 100190, China; School of Physical Sciences, University of Chinese Academy of Sciences, Beijing 100049, China*

Zhiwei Hu − *Max Planck Institute for Chemical Physics of Solids, 01187 Dresden, Germany;* orcid.org/0000-0003-0324-2227

Hong-Ji Lin – *National Synchrotron Radiation Research Center, Hsinchu 300092, Taiwan*

Chien-Te Chen – *National Synchrotron Radiation Research Center, Hsinchu 300092, Taiwan*

Qingbo Meng – *Beijing National Laboratory for Condensed Matter Physics, Institute of Physics, Chinese Academy of Sciences, Beijing 100190, China; Songshan Lake Materials Laboratory, Dongguan, Guangdong 523808, China;* orcid.org/0000-0003-4531-4700

Pu Yu – *State Key Laboratory of Low Dimensional Quantum Physics and Department of Physics, Tsinghua University, Beijing 100084, China;* orcid.org/0000-0002-5513-7632

Complete contact information is available at:
https://pubs.acs.org/10.1021/acs.inorgchem.3c03288

Author Contributions

The manuscript was written through contributions of all authors.

Notes

The authors declare no competing financial interest.

■ ACKNOWLEDGMENTS

This work was supported by the National Key R&D Program of China (Grant No. 2021YFA1400300), the Beijing Natural Science Foundation (Grant No. Z200007), the National Natural Science Foundation of China (Grant Nos. 11934017, 12261131499, 11921004, 12274361), the Chinese Academy of Sciences (Grant No. XDB33000000), the Natural Science Foundation of Jiangsu Province (BK20211361), and the College Natural Science Research Project of Jiangsu Province (20KJA430004). We acknowledge support from the Max Planck-POSTECH-Hsinchu Center for Complex Phase Materials.

■ REFERENCES

(1) Takei, S.; Tserkovnyak, Y. Superfluid spin transport through easy-plane ferromagnetic insulators. *Phys. Rev. Lett.* **2014**, *112*, No. 227201.

(2) Kawabata, S.; Asano, Y.; Tanaka, Y.; Golubov, A. A.; Kashiwaya, S. Josephson pi state in a ferromagnetic insulator. *Phys. Rev. Lett.* **2010**, *104*, No. 117002.

(3) Ojajärvi, R.; Heikkilä, T. T.; Virtanen, P.; Silaev, M. A. Giant enhancement to spin battery effect in superconductor/ferromagnetic insulator systems. *Phys. Rev. B* **2021**, *103*, No. 224524.

(4) Katmis, F.; Lauter, V.; Nogueira, F. S.; Assaf, B. A.; Jamer, M. E.; Wei, P.; Satpati, B.; Freeland, J. W.; Eremin, I.; Heiman, D.; Jarillo-Herrero, P.; Moodera, J. S. A high-temperature ferromagnetic topological insulating phase by proximity coupling. *Nature* **2016**, *533*, 513.

(5) Ferreira, G. J.; Loss, D. Magnetically defined qubits on 3D topological insulators. *Phys. Rev. Lett.* **2013**, *111*, No. 106802.

(6) Li, Y.; Li, B. Z.; Zhang, W. S.; Dai, D. S. Tunneling conductance and magnetoresistance of ferromagnet/ferromagnetic insulator (semiconductor)/ferromagnet junctions. *Phys. Rev. B* **1998**, *57*, 1079.

(7) Jiang, S.; Li, L.; Wang, Z.; Shan, J.; Mak, K. F. Spin tunnel field-effect transistors based on two-dimensional van der Waals heterostructures. *Nat. Electron.* **2019**, *2*, 159.

(8) Millis, A. J.; Shraiman, B. I.; Mueller, R. Dynamic Jahn-Teller effect and colossal magnetoresistance in $La_{1-x}Sr_xMnO_3$. *Phys. Rev. Lett.* **1996**, *77*, 175.

(9) Matsukura, F.; Ohno, H.; Shen, A.; Sugawara, Y. Transport properties and origin of ferromagnetism in (Ga,Mn)As. *Phys. Rev. B* **1998**, *57*, R2037.

(10) Mahadevan, P.; Kumar, A.; Choudhury, D.; Sarma, D. D. Charge ordering induced ferromagnetic insulator: $K_2Cr_8O_{16}$. *Phys. Rev. Lett.* **2010**, *104*, No. 256401.

(11) Erickson, A. S.; Misra, S.; Miller, G. J.; Gupta, R. R.; Schlesinger, Z.; Harrison, W. A.; Kim, J. M.; Fisher, I. R. Ferromagnetism in the Mott insulator Ba_2NaOsO_6. *Phys. Rev. Lett.* **2007**, *99*, No. 016404.

(12) Lee, J. H.; Fang, L.; Vlahos, E.; Ke, X.; Jung, Y. W.; Kourkoutis, L. F.; Kim, J. W.; Ryan, P. J.; Heeg, T.; Roeckerath, M.; Goian, V.; Bernhagen, M.; Uecker, R.; Hammel, P. C.; Rabe, K. M.; Kamba, S.; Schubert, J.; Freeland, J. W.; Muller, D. A.; Fennie, C. J.; Schiffer, P.; Gopalan, V.; Johnston-Halperin, E.; Schlom, D. G. A strong ferroelectric ferromagnet created by means of spin-lattice coupling. *Nature* **2010**, *466*, 954.

(13) Matthias, B. T.; Bozorth, R. M.; Van Vleck, J. H. Ferromagnetic Interaction in EuO. *Phys. Rev. Lett.* **1961**, *7*, 160.

(14) Müller, W.; Nolting, W. Temperature-dependent quasiparticle band structure of the ferromagnetic semiconductor EuS. *Phys. Rev. B* **2002**, *66*, No. 085205.

(15) McGuire, M. A.; Dixit, H.; Cooper, V. R.; Sales, B. C. Coupling of Crystal Structure and Magnetism in the Layered, Ferromagnetic Insulator CrI_3. *Chem. Mater.* **2015**, *27*, 612.

(16) Zhang, Z.; Shang, J.; Jiang, C.; Rasmita, A.; Gao, W.; Yu, T. Direct Photoluminescence Probing of Ferromagnetism in Monolayer Two-Dimensional $CrBr_3$. *Nano Lett.* **2019**, *19*, 3138.

(17) Williams, T. J.; Aczel, A. A.; Lumsden, M. D.; Nagler, S. E.; Stone, M. B.; Yan, J. Q.; Mandrus, D. Magnetic correlations in the quasi-two-dimensional semiconducting ferromagnet $CrSiTe_3$. *Phys. Rev. B* **2015**, *92*, No. 144404.

(18) Gong, C.; Li, L.; Li, Z.; Ji, H.; Stern, A.; Xia, Y.; Cao, T.; Bao, W.; Wang, C.; Wang, Y.; Qiu, Z. Q.; Cava, R. J.; Louie, S. G.; Xia, J.; Zhang, X. Discovery of intrinsic ferromagnetism in two-dimensional van der Waals crystals. *Nature* **2017**, *546*, 265.

(19) Rogado, N. S.; Li, J.; Sleight, A. W.; Subramanian, M. A. Magnetocapacitance and Magnetoresistance Near Room Temperature in a Ferromagnetic Semiconductor: La_2NiMnO_6. *Adv. Mater.* **2005**, *17*, 2225.

(20) Feng, H. L.; Calder, S.; Ghimire, M. P.; Yuan, Y.-H.; Shirako, Y.; Tsujimoto, Y.; Matsushita, Y.; Hu, Z.; Kuo, C.-Y.; Tjeng, L. H.; Pi, T.-W.; Soo, Y.-L.; He, J.; Tanaka, M.; Katsuya, Y.; Richter, M.; Yamaura, K. Ba_2NiOsO_6: A Dirac-Mott insulator with ferromagnetism near 100 K. *Phys. Rev. B* **2016**, *94*, No. 235158.

(21) Kimura, T.; Kawamoto, S.; Yamada, I.; Azuma, M.; Takano, M.; Tokura, Y. Magnetocapacitance effect in multiferroic $BiMnO_3$. *Phys. Rev. B* **2003**, *67*, No. 180401.

(22) Shamoto, S.-i.; Ito, T. U.; Onishi, H.; Yamauchi, H.; Inamura, Y.; Matsuura, M.; Akatsu, M.; Kodama, K.; Nakao, A.; Moyoshi, T.; Munakata, K.; Ohhara, T.; Nakamura, M.; Ohira-Kawamura, S.; Nemoto, Y.; Shibata, K. Neutron scattering study of yttrium iron garnet. *Phys. Rev. B* **2018**, *97*, No. 054429.

(23) Moodera, J. S.; Santos, T. S.; Nagahama, T. The phenomena of spin-filter tunnelling. *J. Phys.: Condens. Matter* **2007**, *19*, No. 165202.

(24) Liu, Z.; Zhang, S.; Wang, X.; Ye, X.; Qin, S.; Shen, X.; Lu, D.; Dai, J.; Cao, Y.; Chen, K.; Radu, F.; Wu, W. B.; Chen, C. T.; Francoual, S.; Mardegan, J. R. L.; Leupold, O.; Tjeng, L. H.; Hu, Z.; Yang, Y. F.; Long, Y. Realization of a Half Metal with a Record-High Curie Temperature in Perovskite Oxides. *Adv. Mater.* **2022**, *34*, No. 2200626.

(25) Larson, A. C.; Von Dreele, R. B. *General Structure Analysis System (GSAS) Report No. LAUR 86–748*; Los Alamos National Laboratory: Los Alamos, NM, 1994.

(26) Kresse, G.; Hafner, J. Ab initio molecular dynamics for liquid metals. *Phys. Rev. B* **1993**, *47*, 558.

(27) Perdew, J. P.; Burke, K.; Ernzerhof, M. Generalized gradient approximation made simple. *Phys. Rev. Lett.* **1996**, *77*, 3865.

(28) Wang, L.; Maxisch, T.; Ceder, G. Oxidation energies of transition metal oxides within the GGA+U framework. *Phys. Rev. B* **2006**, *73*, No. 195107.

(29) Monkhorst, H. J.; Pack, J. D. Special points for Brillonin-zone integrations. *Phys. Rev. B* **1976**, *13*, 5188.

(30) Heyd, J.; Scuseria, G. E.; Ernzerhof, M. Hybrid functionals based on a screened Coulomb potential. *J. Chem. Phys.* **2003**, *118*, 8207.

(31) Heyd, J.; Scuseria, G. E.; Ernzerhof, M. Hybrid functionals based on a screened Coulomb potential. *J. Chem. Phys.* **2006**, *124*, 219906.

(32) Blochl, P. E.; Jepsen, O.; Andersen, O. K. Improved tetrahedron method for Brillouin-zone integrations. *Phys. Rev. B* **1994**, *49*, 16223.

(33) Vasil'ev, A. N.; Volkova, O. S. New functional materials $AC_3B_4O_{12}$ (Review). *Low Temp. Phys.* **2007**, *33*, 895.

(34) Burnus, T.; Hu, Z.; Wu, H.; Cezar, J. C.; Niitaka, S.; Takagi, H.; Chang, C. F.; Brookes, N. B.; Lin, H. J.; Jang, L. Y.; Tanaka, A.; Liang, K. S.; Chen, C. T.; Tjeng, L. H. X-ray absorption and x-ray magnetic dichroism study on Ca_3CoRhO_6 and Ca_3FeRhO_6. *Phys. Rev. B* **2008**, *77*, No. 205111.

(35) Nemrava, S.; Vinnik, D. A.; Hu, Z.; Valldor, M.; Kuo, C.-Y.; Zherebtsov, D. A.; Gudkova, S. A.; Chen, C.-T.; Tjeng, L. H.; Niewa, R. Three Oxidation States of Manganese in the Barium Hexaferrite $BaFe_{12-x}Mn_xO_{19}$. *Inorg. Chem.* **2017**, *56*, 3861.

(36) McGuinness, C.; Downes, J. E.; Sheridan, P.; Glans, P. A.; Smith, K. E.; Si, W.; Johnson, P. D. X-ray spectroscopic study of the electronic structure of the high-dielectric-constant material $CaCu_3Ti_4O_{12}$. *Phys. Rev. B* **2005**, *71*, No. 195111.

(37) Burnus, T.; Hu, Z.; Hsieh, H. H.; Joly, V. L. J.; Joy, P. A.; Haverkort, M. W.; Wu, H.; Tanaka, A.; Lin, H. J.; Chen, C. T.; Tjeng, L. H. Local electronic structure and magnetic properties of $LaMn_{0.5}Co_{0.5}O_3$ studied by x-ray absorption and magnetic circular dichroism spectroscopy. *Phys. Rev. B* **2008**, *77*, No. 125124.

(38) Retuerto, M.; Skiadopoulou, S.; Li, M. R.; Abakumov, A. M.; Croft, M.; Ignatov, A.; Sarkar, T.; Abbett, B. M.; Pokorny, J.; Savinov, M.; Nuzhnyy, D.; Prokleska, J.; Abeykoon, M.; Stephens, P. W.; Hodges, J. P.; Vanek, P.; Fennie, C. J.; Rabe, K. M.; Kamba, S.; Greenblatt, M. Pb_2MnTeO_6 Double Perovskite: An Antipolar Antiferromagnet. *Inorg. Chem.* **2016**, *55*, 4320.

(39) Smart, J. S. The Néel Theory of Ferrimagnetism. *Am. J. Phys.* **1955**, *23*, 356.

(40) Li, B.; Ye, X.; Wang, X.; Zhang, J.; Lu, D.; Zhao, H.; Pi, M.; Hu, Z.; Lin, H. J.; Chen, C. T.; Pan, Z.; Qin, X.; Long, Y. High-Pressure-Stabilized Post-Spinel Phase of $CdFe_2O_4$ with Distinct Magnetism from Its Ambient-Pressure Spinel Phase. *Inorg. Chem.* **2023**, *62*, 9139.

(41) Liu, Z.; Wang, X.; Ye, X.; Shen, X.; Bian, Y.; Ding, W.; Agrestini, S.; Liao, S.-C.; Lin, H.-J.; Chen, C.-T.; Weng, S.-C.; Chen, K.; Ohresser, P.; Nataf, L.; Baudelet, F.; Sheng, Z.; Francoual, S.; Mardegan, J. R. L.; Leupold, O.; Li, Z.; Xi, X.; Wang, W.; Tjeng, L. H.; Hu, Z.; Long, Y. Observation of A site antiferromagnetic and B site ferrimagnetic orderings in the quadruple perovskite oxide $CaCu_3Co_2Re_2O_{12}$. *Phys. Rev. B* **2021**, *103*, No. 014414.

(42) Zhang, J.; Shi, F.; Lin, J.; Chen, D.; Gao, J.; Huang, Z.; Ding, X.; Tang, C. Self-assembled 3-D architectures of BiOBr as a visible light-driven photocatalyst. *Chem. Mater.* **2008**, *20*, 2937.

(43) Steeneken, P. G.; Tjeng, L. H.; Elfimov, I.; Sawatzky, G. A.; Ghiringhelli, G.; Brookes, N. B.; Huang, D. J. Exchange splitting and charge carrier spin polarization in EuO. *Phys. Rev. Lett.* **2002**, *88*, No. 047201.

(44) Webster, L.; Yan, J.-A. Strain-tunable magnetic anisotropy in monolayer $CrCl_3$, $CrBr_3$, and CrI_3. *Phys. Rev. B* **2018**, *98*, No. 144411.

(45) Senn, M. S.; Chen, W.-t.; Saito, T.; García-Martín, S.; Attfield, J. P.; Shimakawa, Y. B-Cation Order Control of Magnetism in the 1322 Perovskite $CaCu_3Fe_2Nb_2O_{12}$. *Chem. Mater.* **2014**, *26*, 4832.

(46) Byeon, S. H.; Lee, S. S.; Parise, J. B.; Woodward, P. M.; Hur, N. H. New ferrimagnetic oxide $CaCu_3Cr_2Sb_2O_{12}$: High-pressure synthesis, structure, and magnetic properties. *Chem. Mater.* **2005**, *17*, 3552.